Design Using Finite Element Analysis of a Switched Reluctance Motor for Electric Vehicle

Kazuhiro Ohyama*, Maged Naguib F. Nashed†, Kenichi Aso*, Hiroaki Fujii** and Hitoshi Uehara**

*Electrical Dep., Fukuoka Institute of Technology, Fukuoka, Japan
†Power Electronics & Energy Conversion Dep., Electronics Research Institute (ERI), Egypt
**Meiwa Manufacturing Co., Ltd, Fukuoka, Japan

ABSTRACT

In this paper, a Switched Reluctance Motor (SRM) employed in an electric vehicle (EV) is designed using the finite element method (FEM). The static torque of the SRM is estimated through magnetic field analysis. The SRM temperature rise over operation time is estimated through heat transfer analysis. First, static torque and temperature rise over the time of 600W SRM is included in the experiment set, and are compared with the calculated results using the FEM under the same conditions. The validity of the magnetic field analysis and heat transfer analysis is verified by the comparisons. In addition, a 60 [kW] SRM employed in an EV, whose output characteristics are equal to a 1500 [cc] gasoline engine, is designed under magnetic field analysis and heat transfer analysis.

Keywords: Switched Reluctance Motor (SRM), PI Current and Speed Controls, and Turn-off control

1. Introduction

The rapid development of automotive technologies has led to serious environmental problems such as petroleum depletion, global warming by CO_2 and air pollution by NOx. As a solution, increased use of high mileage automobiles and low emissions vehicle, such as in hybrid vehicles (HV) is necessary. However, the use of HVs has not caught on yet. This is because the price of HVs is still higher than the price of gasoline-powered vehicles (GV) of equal power.

Switched reluctance motor (SRM) rotates by a reluctance torque, which originates from the change of the resistance of the magnetic circuit. The stator and rotor have salient pole structures, made from laminated non-oriented electrical steel. The concentrated winding coils are installed only in the stator. The SRM is known for its low cost. Its structure is simpler in design than those in induction motors or synchronous motors, since its rotor has winding coils or permanent magnets. Therefore, SRMs have the possibility of withstanding high-speed rotations and operating at high temperatures and under inferior road surface conditions by absorbing impact and vibrations[1].

The main problems with SRMs include high torque pulsation and noise. However, those problems are being solved by development of the power electronics and improvement in the technology[2]. Basic performance

improvements of SRM drives have contributed to its extension in the application field and have led to the examination and application of SRMs in electric vehicles (EVs). Research institutes have already made reports on the design of SRMs for EVs and on performance enhancement of control methods for SRM applications for EVs.

In one project, researchers are currently studying SRMs in EVs with power performance equivalent to 1500[cc] GV. In this project, a low cost SRM with solid features is chosen with a design suitable for the dimensions and power of an EV. The following goals are used as design guidelines: equivalent output characteristics of 1500cc gasoline engines, smaller size and lighter SRMs. In the case of FFs(front engine front-wheel drive systems) two SRMs are used in order to omit the differential gear.

In this paper, the design process of a SRM for EV is reported through magnetic field analysis and heat transfer analysis of finite element method (FEM). To the authors' knowledge, there are currently no other reports on designed SRMs for EVs using the analysis of FEM. First, the static torque and temperature rise over a time of 600W in the model SRM were measured and compared with the calculated results using the FEM under the same conditions. The validity of magnetic field analysis and

heat transfer analysis was verified by the comparisons. Hence, the SRM design procedure, using both analysis results, was explained. Finally, an SRM for EVs, with output characteristics which are equivalent to a 1500cc gasoline engine, was designed.

2. Static Torque

2.1 Calculation of Static Torque

Inductance and static torque of the 600W SRM model were calculated using ANSYS software of FEM. Fig. 1 shows the analytical model of the SRM. Table 1 shows the condition of analysis. Table 2 shows the specifications of the SRM. Using the analytical model, as shown in Fig. 1, the calculation is made through a two-dimensional static magnetic field analysis.

In this analysis, a three-phase SRM which has a six pole stator and a four pole rotor was used. Since the pole number of the rotor is four, the magnetic circuit becomes the same after rotating 90 degrees, when only one phase is excited. In addition, the stator salient pole and rotor salient pole repeat in facing conditions and non-facing conditions at a 45 degree rotation interval. It is possible to obtain the inductance of a 360 degree rotation by using the calculated inductance of the 45 degree rotations due to the geometric symmetry. At that point, the non-facing condition of the
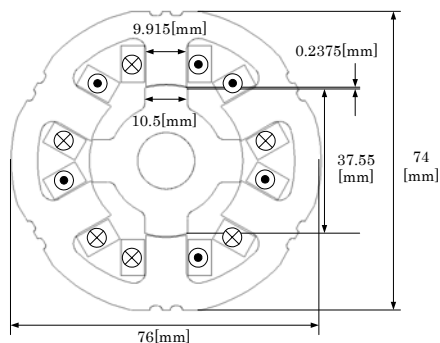

Fig. 1 Analytical model

Table 1 Condition of Analysis

Number of node	15173
Number of element	7636
Mesh size	0.0013
Shape of element	triangle
Excitation phase of coil	one phase only
Magnetomotive force	80 [AT]
Current density	$1.559*10^6[A/m^2]$
Partial area of coil	51.3 [mm^2]
Analysis range	0-45 [deg]

Table 2 Specification of SRM

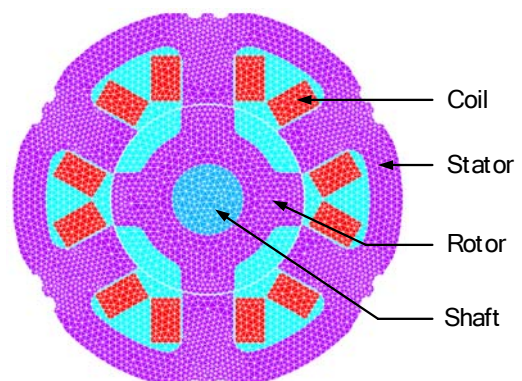| stator outer diameter	76 [mm]
rotor outer diameter	37.55 [mm]
output	600 [W]
air gap	0.2375 [mm]
stack length	50 [mm]
number of windings/pole	20 [turns/pole]
stator/rotor poles	6/4

Fig. 2 Element distribution

stator salient pole and rotor salient pole is defined as 0 degrees, and the rotor is made to rotate 45 degrees of the facing condition. For each degree, the inductance and static torque of one phase are calculated.

At rotor position θ, the magnetic co energy W'(θ) is calculated according to the following equation: while the rotor is made to rotate from 0 degrees to 45 degrees for each degree.

$$W'(\theta) = \frac{1}{2} \sum_i \frac{B_i^2}{\mu_i} v_i \tag{1}$$

Where Bi is the magnetic flux density of each element, μi is the permeability of each element, and vi is the volume of each element.

Inductance L(θ) in rotor position θ is calculated according to the following equation.

$$L(\theta) = \frac{2W'(\theta)}{i^2} \tag{2}$$

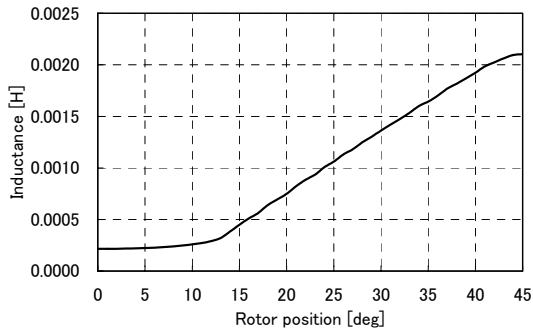Where i is the excitation current.

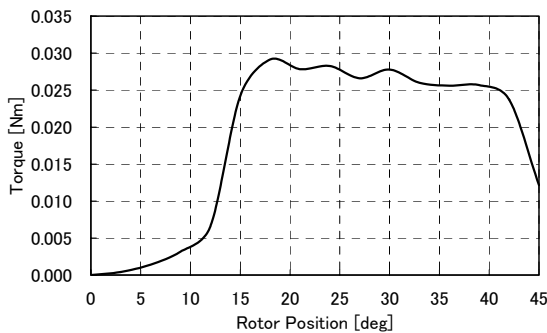Fig. 3 shows the inductance L(θ) in rotor position θ calculated using equations (1) and (2).

Using the W'(θ) or L(θ), the reluctance torque T(θ) is calculated according to the following equation.

$$T(\theta) = \frac{\partial W'(\theta)}{\partial \theta} = \frac{1}{2} i^2 \frac{dL(\theta)}{d\theta} \tag{3}$$

Fig. 4 shows the static torque T(θ) in rotor position θ calculated by using equation (3). T(θ) of the positive direction is obtained regardless of the current direction. If the exciting current is flowing when L(θ) increases then T(θ) is proportional to the derivative for the rotor position of the inductance. In short, the rotor keeps rotating in the positive direction because the torque of the positive direction is obtained at every excitation. When the winding is continually excited, the gradient of L(θ) moves in a positive direction.
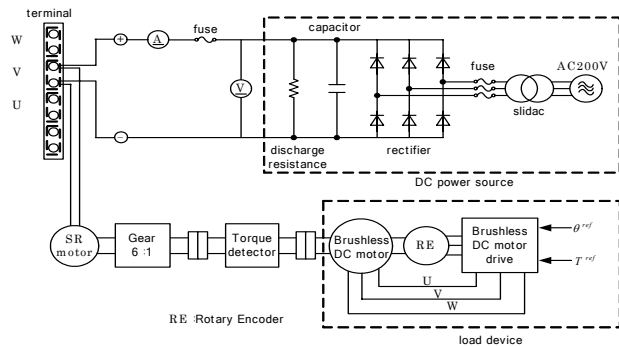

Fig. 3 Calculated results of inductance

Fig. 5 Experiment circuit

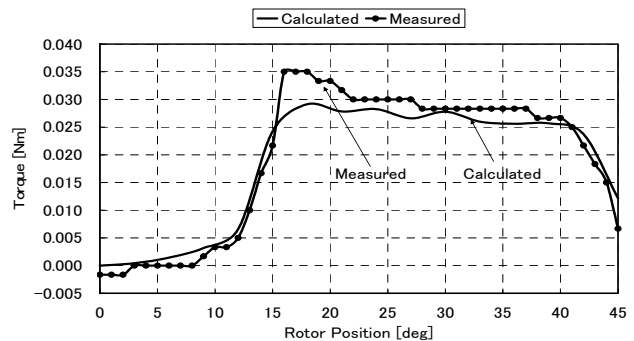Fig. 4 Calculated results of static torque

Fig. 6 Comparison of calculated results and experimental results of Static torque

2.2 Experimental Results

The static torque while exciting only one phase was measured using the 600W SRM model. Fig. 5 shows the experiment circuit. The excitation current is applied to the one phase of the SRM using the DC power source while the static torque at rotor position θ was measured using the torque meter. The rotor position of the SRM was fixed using a brushless DC motor drive. The rotor position of the SRM can be fixed by controlling the rotor position of the brushless DC motor using the brushless DC motor drive. There is a speed reducer between the brushless DC motor and SRM. The gear ratio is 6:1. Therefore, it is possible to rotate the SRM one degree by giving the command signal, which rotates the brushless DC motor drive 1/6 of a degree. The static torque, in the position fixed by the brushless DC motor drive, can be measured using the torque meter. The comparison of calculated and experimental results of the static torque is shown in Fig. 6. The static torque, calculated by magnetic field analysis, concurs with the experimental result measured under the same condition. Therefore, the validity of the magnetic field analysis using FEM utilized for the design was proven.

3. Heat Transfer Analysis

3.1 Calculation of Static Torque

Heat transfer analysis is carried out using the analytical model shown in Fig. 1. However, in the actual analytical model used, in order to choose the condition equal to that of experiment, the rotor was removed.

The heat quantity of the coil must be proven in order to carry out the heat transfer analysis through the magnetic field. During magnetic field analysis, the voltage drop across the stator coils occurs at excitation phase, and the Joule heat per unit cube product of the coil is calculated. The Joule heat obtained during the magnetic field analysis is set at the coils at which point the heat transfer analysis is carried out.

The heat transfer between the SRM and the outside air is done by natural convection. The heat transfer coefficient in natural convection was obtained from the simple formula for heat transfer of natural convection [15]. In the stator surface, where its contact plane with the air is smooth, the simple formula for the laminar flow shown in

Table 3 Material Property

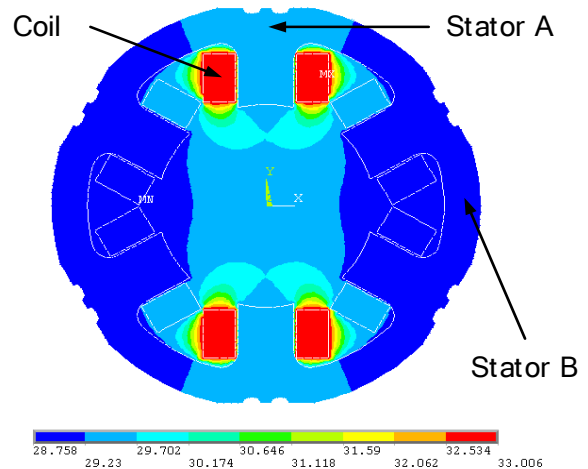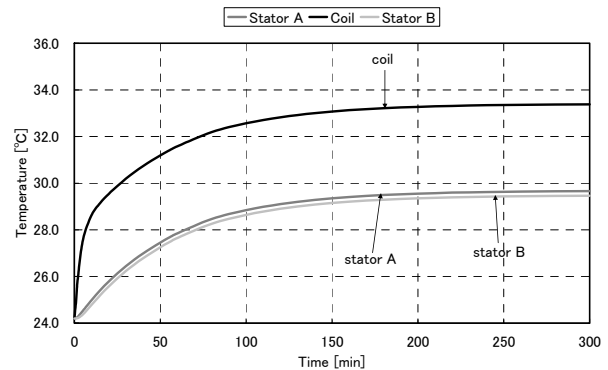| Material	Temperature [℃]	Density [kg/m³]	Specific Heat [J/Kg·K]	Termal Conductivity [W/m·K]
Coil(Copper)	20	8950	0.383×10^3	386
	100		0.398×10^3	379
	300		0.425×10^3	369
Silicon Steal	20	7770	0.460×10^3	42
Air (1atm300K)	27	1.1763	1.007×10^3	0.02614

Fig. 7 Temperature distribution after 120 minutes

Fig. 8 Calculated results of temperature rise

the following equation is used.

$$\alpha = 1.42 \times \left(\frac{\Delta t}{l}\right)^{\frac{1}{4}}$$

(4)

Where, α is a heat transfer coefficient, Δt is a gradient of temperature change, and l is the core thickness. The simple formula for the turbulent flow, as shown in the equation, is used on the coil surface without smooth air contact.

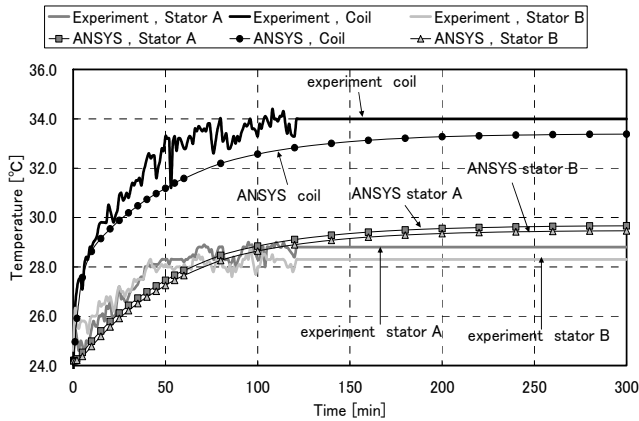$$\alpha = 0.95 \times (\Delta t)^{\frac{1}{3}}$$

(5)

Fig. 9 Comparison of experimental results and calculated results of temperature rise

The initial value of the temperature gradient Δt used in equations (4) and (5) is assumed to be 0[K]. The α is calculated for a fixed time and it is renewed as time passes on the boundary surface. In this analysis, the temperature is measured every five minutes for a total interval of one hour. The measured temperature rise was large. It was noted that after the initial hour after 20 minutes the temperature approached a steady state, i.e. the temperature change decreases.

Fig. 7 shows the temperature distribution after two hours of applying 10[A] for only one phase. Fig. 8 shows the temperature rise in the coil and stator during the two hours. The positions, where the temperature rises, see Fig. 8, were observed in three places shown in Fig. 7. The first place is on the coil surface during the excitation phase, and the other two places are on the stator surface. Point A is at the base of the stator salient pole division of the excitation phase. Point B is at the stator surface and is situated furthest away from the excitation phase.

3.2 Experimental Results

In the heat transfer analysis in 3.1, of the SRM stator model, the temperature change of the coil and stator was measured during only one excitation phase. The applied excitation current of 10[A] was the same condition of the heat transfer. Using a radiation thermometer, the temperature of the coil and stator was measured every minute. The emissivity of the radiation thermometer was 0.86. The room temperature in the experiment was 24.2 [degrees centigrade]. Fig. 9 shows a comparison of

experimental results and calculated results of temperature rise. The continuous line shows the calculated results while the plotted line shows the experimental results. The thermometry was carried out at the same three places as in the heat transfer analysis.

The experimental results and calculated results reached an equilibrium state at about two hours, as is shown in Fig. 9. The calculated results are lower, by 1.0[degree centigrade], than the experimental results of the coil temperature. The experimental results rise by only about 1.0[degree centigrade] more than the calculated results of the stator temperature. The calculated results of temperature rise of the coil during heat transfer analysis tends to decrease further than experimental results. The heat transfer analysis using FEM produced an error in the experimental result. Nevertheless, sufficient accuracy required for the design can be ensured by considering safety factors. Hence, heat transfer analysis of the SRM for EV was carried out using a fixed value (α = 1.0) which considers safety factors.

4. Design Of SRM for EV

4.1 Dimension of SRM and moderating ratio

Considering engine room space in a base car, the stator diameters of 250, 300, and 350[mm] are likely candidates and stator depths of 150, 200, and 250[mm] are examined for diameter size. The shape of rotor and stator was decided according to reference[16]. Fig. 10 shows an analytical model for the stator diameter of 350[mm]. Table 4 shows the conditions of analysis. Table 5 shows the specifications of the SRM. The SRM is designed at 60 [kW] in order to obtain output characteristics equal to 1500cc class gasoline engines. Assuming the utilization of two SRMs, in order to omit the differential gear, an SRM of 30[kW] was designed.

Large torque is required for an EV to start. Table 6 shows the average total torque of the two designed SRMs. The average torque is the total of the three-phases. The average torque without using a speed reducer, shown in Table 6, is much smaller than the torque performance obtained in the curve of gasoline engines, as shown in Fig. 10. With this fact in mind, it is clear that a speed reducer is necessary. Thus a speed reducer was established between the SRM and driving shafts. The speed reducer

used here has only one ratio and is not a change gear which used in gasoline vehicles(GV).

The reducer is also beneficial for acceleration from a resting state due to the fact that when torque increases, the moderating ratio also increases and the maximum speed lowers. As the dimensions of the gearbox increases, it can not fit into the engine room space. Thus, the optimum moderating ratio of 1/5 is adopted. Starting torque and performance of high speed operation are equivalent to those in GVs. Table 7 shows the average total torque of two SRMs with a moderating ratio of 1/5. The average torques which are equivalent to the peak torque of GVs are obtained under the following conditions: a depth of 250 [mm] and diameter of 300[mm], and the depths of 200 and 250[mm] for the for a diameter of 350[mm]. Considering

Fig. 10 Analytical model for stator diameter of 350 [mm]

Fig. 11 Temperature distribution after 120 minutes

Table 4 Condition of Analysis

stator outer diameter	250 [mm]	300 [mm]	350 [mm]
number of node	11377~11785	11481~11849	11945~12633
number of element	5598~5802	5650~5834	5866~6210
mesh size (all area)	0.0055	0.0065	0.0070
shape of element	triangle	triangle	triangle
excitation phase of coil	one phase only	one phase only	one phase only
excitation current	100 [A]	100 [A]	100 [A]
current density	8.4669×10^6 [A/m²]	8.3819×10^6 [A/m²]	8.4560×10^6 [A/m²]
partial area of coil	555.10 [mm²]	799.34 [mm²]	1087.99[mm²]
analysys range	0~45 [deg]	0~45 [deg]	0~45 [deg]

the shape of the engine room space at the car's base, there are no depth allowances. Therefore, diameters of 350 [mm] and depth of 200[mm] were selected.

Only static torque, which arises when constant current is applied in rest state, has been examined until now. However, the generated torque decreases, because the delay occurs in the stator current, when the rotational frequency of SRM rises. Dynamic simulation with consideration of the electrical characteristic of the coil and mechanical system are necessary to examine the generated torque in general transit. The generated torque in general transit time will be examined in the next project.

4.2 Calculation of Temperature Rise

The temperature rise of the SRM under continuous operation at the rated current of 100 [A] was observed. In the rated operation, the temperature of the coil was not allowed to go over 140[degrees centigrade]. The heat transfer analysis by applying a current of 100[A] to the coil for one hour was carried out, and the temperature rise of the coil and stator was observed.
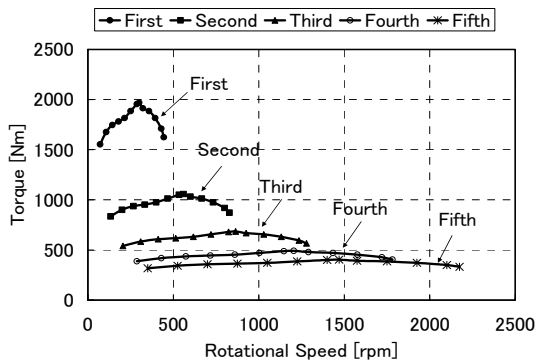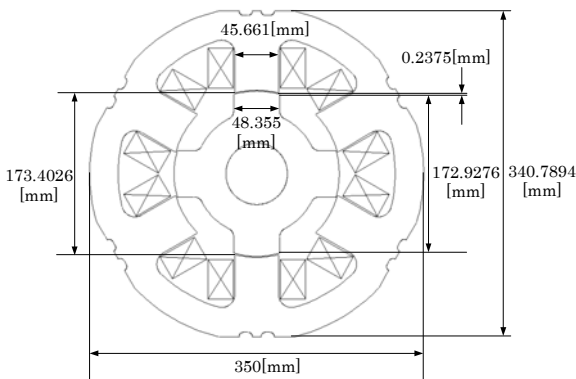
Table 5 Specification of SRM

stator outer diameter	250 [mm]	300 [mm]	350 [mm]
rotor outer diameter	123.5197 [mm]	148.2236 [mm]	172.9276 [mm]
output	30 [kW]×2	30 [kW]×2	30 [kW]×2
air gap	0.2375 [mm]	0.2375 [mm]	0.2375 [mm]
stack length	150, 200, 250 [mm]	150, 200, 250 [mm]	150, 200, 250 [mm]
number of windings/pole	47 [turns/pole]	67 [turns/pole]	92 [turns/pole]
stator/rotor poles	6/4	6/4	6/4

Table 6 Average Torque

Motor size [cm]	stack length [cm]	Excitation Current [A]	3 phase Average Torque [Nm]
25	15	100	148.45123
	20	100	197.93497
	25	100	247.41871
30	15	100	238.94170
	20	100	318.58893
	25	100	398.23616
35	15	100	356.26735
	20	100	475.02313
	25	100	593.77892

Table 7 Average Torque Considering Moderating Ratio

Motor size [cm]	stack length [cm]	Excitation Current [A]	3 phase Average Torque [Nm]
25	15	100	742.25613
	20	100	989.67484
	25	100	1237.09356
30	15	100	1194.70848
	20	100	1592.94464
	25	100	1991.18080
35	15	100	1781.33675
	20	100	2375.11567
	25	100	2968.89458

The analysis was carried out using the analytical model which added a cooling system to the analytical model of Fig. 11. Fig. 12 shows the element distribution of the analytical model with the added cooling system. The analysis was carried out using a copper pipe with water as a cooling system. The copper pipe was used as a cooling system and the water was used as a refrigerant. The shape of the copper pipe was a column with a 4[mm] outer diameter and 12[mm] inner diameter.

The initial temperature difference was set at 0 when the calculation was started. Heat transfer coefficient α is renewed and as time passed the temperature gradient rose. However, the constant value α = 1.0[W/m2K], as a safety factor, was used for the stator surface in this analysis, since the calculation time is shortened. Temperature is calculated by comparing α during temperature change. The temperature rises when using constant value α = 1.0[W/m2K]. The cooling was done by a forced convection of water passing through copper pipes within the stator. The general value of the average heat transfer coefficient for the water flow inside the cylinder is 6000 [W/m2K][17]. At that point, α = 6000[W/m2K] was set for the water in the copper pipe in this analysis. The air gap of the SRM is an aerial forced convection, since the rotor rotates. The average heat transfer coefficient of the aerial forced convection in the cylinder is 50[W/m2K] [17]. However, the interior of the SRM is not exactly a cylinder. The heat transfer coefficient of the SRM interior is 30[W/m2K], which is a middle value of the average heat transfer coefficient 6[W/m2K] found in natural convection and is an average heat transfer coefficient 50[W/m2K] in forced convection.

The current was applied to each coil according to the order of the excitation timing. It was assumed that the three-phase current flows simultaneously, because the excitation phase is switched at high speed. The current of 100 [A] per phase flowed instantaneously. The rms value of this current is 57.74[A] per phase assuming that the current of three-phase is flowing simultaneously.

Fig. 13 shows the temperature distribution. The temperature after 60 minutes was 62.2[degrees centigrade]. Moreover, it was confirmed that the temperature reached an equilibrium state from Fig. 14. The temperature of the coil did not exceed 140[degrees centigrade] which is an allowable temperature, even if the rated current of 100[A]

is applied for an hour. Therefore, it can be confirmed that the coil can resist heat sufficiently, even if the rated

Table 8 Material Property

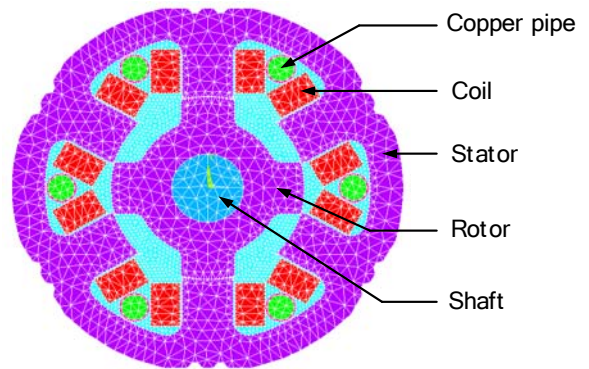| Material	Temperature [℃]	Density [kg/m³]	Specific Heat [J/Kg·K]	Termal Conductivity [W/m·K]
Coil·copper pipe (Copper)	20	8950	0.383×10^3	386
	100		0.398×10^3	379
	300		0.425×10^3	369
Silicon Steal	20	7770	0.460×10^3	42
Iron	20	7830	0.465×10^3	54
Water	20	998.2	4.183×10^3	0.602
Air (1atm,300K)	27	1.1763	1.007×10^3	0.02614

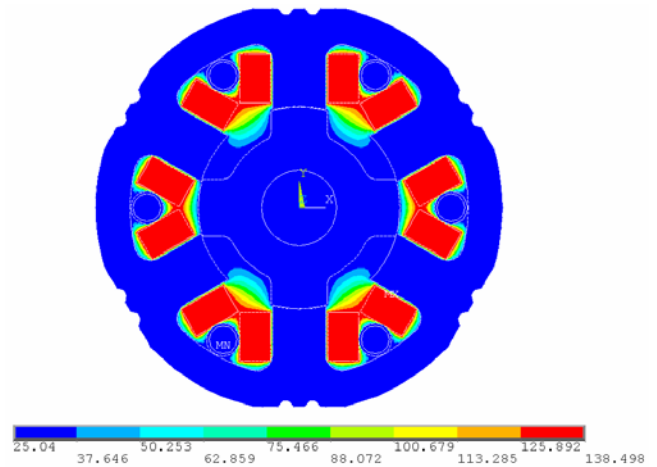Fig. 12 Element distribution

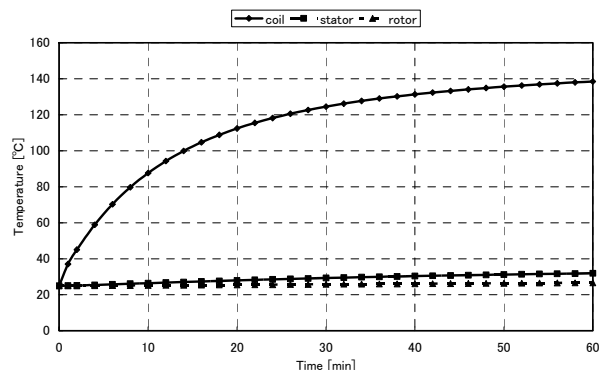Fig. 13 Temperature distribution

Fig. 14 Temperature distribution

continuous operation is carried out.

5. Conclusion

It was confirmed that static torque calculated in magnetic field analysis and temperature rise calculated in heat transfer analysis agreed with the experimental results. Therefore, magnetic field analysis and heat transfer analysis using FEM can be utilized for the design of SRMs.

The SRM for an EV with output characteristics equivalent to output characteristics of a 1500cc GV was designed. In addition, heat transfer analysis was carried out for continuous rating operation. It was confirmed that the temperature of the coil does not exceed 140[degrees centigrade], which is an allowable coil operating temperature.

References

[1] A. Chiba, "Design of a Switched Reluctance Drive and Its Application," J. Magn. Soc. Japan, Vol.26, No.8, 909-914, 2002.

[2] M. Morimoto, N. Matsui, and Y. Takeda, "Recent Advances of Reluctance Motors", IEEJ Trans. IA, Vol.119, No.10, 1145-1148, 1999.

[3] K. M. Rahman, B. Fahimi, G. Suresh, A. V. Rajarathnam, and M. Ehsani, "Application of Switched Reluctance Motor Application to EV and HEV: Design and Control Issues," IEEE Trans. Ind. Applicat., vol. 36, 111-121, January/February, 2000.

[4] S. S. Ramamurthy, and J. B. Balda, "Sizing a Switched Reluctance Motor for Electric Vehicles," IEEE Trans. Ind. Applicat., vol. 37, 1256-1264, 2001.

[5] R. B. Inderka, M. Menne, and R. W. A. A. D. Doncker, "Control of Switched Reluctance Drives for Electric Vehicle Application," IEEE Trans. Ind. Electron., vol. 49, 48-53, 2002.

[6] K. M. Rahman and S. E. Schulz, "Design of High-Efficiency and High-Torque-Density Switched Reluctance Motor for Vehicle Propulsion," IEEE Trans. Ind. Applicat., vol. 38, 1500-1507, 2002.

[7] W. Cai, P. Pillay, Z. Tang, and A. M. Omekanda, "Low-Vibration Design of Switched Reluctance Motors for Vehicle Propulsion Using Model Analysis," IEEE Trans. Ind. Applicat., vol. 39, 971-977, 2003.

[8] Y. Suzuki, K. Nakamura, and O. Ichinokura, "Consideration on Multipolar Switched Reluctance Motors," IEE Japan, RM-03-87, 1-6, 2003.

[9] K. M. Rahman and S. E. Schulz, "High-Performance Fully Digital Switched Reluctance Motor Controller for Vehicle Propulsion," IEEE Trans. Ind. Applicat., vol. 38, 1062-1071, 2002.

[10] M. Omekanda, "A New Technique for Multidimensional Optimization of Switched Reluctance Motors for Vehicle Propulsion," IEEE Trans. Ind. Applicat., vol. 39, 672-676, 2003.

[11] R. B. Inderka and R. W. A. A. D. Doncker, "High-Dynamic Direct Average Torque Control for Switched Reluctance Drives," IEEE Trans. Ind. Applicat., vol. 39, 1040-1045, 2003.

[12] S. E. Schulz and K. M. Rahman, "High-Performance Digital PI Current Regulator for EV Switched Reluctance Motor Drives," IEEE Trans. Ind. Applicat., vol. 39, 1118-1126, 2003.

[13] S. Wang, Q. Zhan, Z. Ma, and L. Zhou, "Implementation of a 50-kW Four-Phase Switched Reluctance Motor Drive System for Hybrid Electric Vehicle," IEEE Trans. Magn., vol. 41, 501-504, 2005.

[14] H. Goto, T. Watanabe, H. Guo, A. Honda, and O. Ichinokura, "Development of an Electric Vehicle with Outer Rotor Type Multipolar Switched Reluctance Motors," IEE Japan, RM-04-54, 2004.

[15] Tanishita, "Heat Transfer Engineering", Shokabo Publishing Co., Ltd., 155-176, 1986.

[16] T. J. E. Miller, "Switched Reluctance Motors and Their Control", Clarendon Pr, 1993.

[17] Nishikawa, Fujita, "Mechanical Engineering Basic Lecture. Heat Transfer Engineering", Rikogakusha Publishing Co., Ltd., 81-82, 1982.

[18] S. Inamura, K. Sawa, "A Study on Temperature Analysis of Switched Reluctance Motor," IEEJ Trans. IA, Vol.123, No.4, 422-428, 2003.

Kazuhiro Ohyama received his B.Eng. degree in Electrical Engineering, M. Eng. and D. Eng. from Kagoshima University, Kagoshima, Japan, in 1993, 1995 and 1998, respectively. He was a visiting scholar at the University of Nottingham, U.K., from 1998 to 1999. In April 1999, he joined the Department of Electrical Engineering, Fukuoka Institute of Technology, as a lecturer. In April 2002, he was promoted to assistant professor. He is currently engaged in the study of motor drives. He is a member of the Institute of Electrical Engineering of Japan.

Maged Naguib Fahmy Nashed received his B.S. degree in Electrical Engineering, from Menoufia University, Egypt, in May 1983, his Diploma of Higher Studies from Cairo University, May 1990, his M.SC. degree in Electrical Engineering, from Ain Shams University, Cairo, Egypt, in April 1995 and his Ph.D. in Electrical Engineering, from Ain Shams University, Cairo, Egypt, in January 2001. He was a researcher for Fukuoka Institute of Technology, Japan, 2005. Since 1989, he has been a researcher with the Department of Power Electronic and Energy Conversion, Electronic Research Institute. He is engaged in research on power electronics, drive circuit, control of drives and renewable energy.

Kenichi Aso received his B. Eng. degree in Electrical Engineering and M. Eng. from Fukuoka Institute of Technology, Fukuoka, Japan, in 2004 and 2006, respectively. He is currently engaged in the study of switched reluctance motor drives. He is a member of the Institute of Electrical Engineering of Japan.

Hiroaki Fujii received his B. Eng. degree in Electrical Engineering from Fukuoka Institute of Technology, Fukuoka, Japan, in 1981. He is currently engaged in the study of switched reluctance motor design.

Hitoshi Uehara received his B. Eng. degree in Electrical Engineering from Fukuoka Institute of Technology, Fukuoka.